A multilayer edge-on single photon counting silicon microstrip detector for innovative imaging techniques in diagnostic radiology

A. Olivo,[a] S. Pani, and D. Dreossi
Dipartimento di Fisica Università di Trieste and INFN, Via A. Valerio 2, 34100 Trieste, Italy

F. Montanari
Sincrotrone Trieste SCpA, Strada Statale 14 km 163.5, 34100 Trieste, Italy

A. Bergamaschi, E. Vallazza, F. Arfelli, R. Longo, L. Rigon, and E. Castelli
Dipartimento di Fisica Università di Trieste and INFN, Via A. Valerio 2, 34100 Trieste, Italy

(Received 29 January 2003; accepted 13 April 2003)

A three-layer detector prototype, obtained by stacking three edge-on single photon counting silicon microstrip detectors, has been developed and widely tested. This was done in the framework of the Synchrotron Radiation for Medical Physics/Frontier Radiology (SYRMEP/FRONTRAD) collaboration activities, whose aim is to improve the quality of mammographic examinations operating both on the source and on the detector side. The active surface of the device has been fully characterized making use of an edge-scanning technique and of a well-collimated laminar synchrotron radiation beam. The obtained data (interlayer distances, channel correspondence, etc.) have then been used to combine information coming from each detector layer, without causing any loss in spatial and contrast resolution of the device. Contrast and spatial resolution have also been separately evaluated for each detector layer. Moreover, imaging techniques (phase contrast, refraction, and scatter imaging), resulting in an increased visibility of low absorbing details, have been implemented, and their effectiveness has been tested on a biological sample. Finally, the possibility of simultaneously acquiring different kind of images with the different detector layers is discussed. This would result in maximizing the information extracted from the sample, while at the same time the high absorption efficiency of the detector device would allow a low dose delivery.
 [DOI: 10.1063/1.1582390]

I. INTRODUCTION

The Synchrotron Radiation for Medical Physics/Frontier Radiology (SYRMEP/FRONTRAD) collaboration has been active for years in the field of digital radiology with synchrotron radiation (SR). The main goal of the collaboration is to optimize the quality of radiological examinations (mammography being the first target), operating both on the source and on the detector side.

On the source side, SR is used in substitution of conventional x-ray tubes. A SR beamline,[1,2] specifically dedicated to mammography, has been built and is currently operated by the collaboration at ELETTRA, the Trieste SR Facility. Compared with a conventional source, SR provides much higher fluxes on a wide range of energies, with the consequent possibility of monochromatizing the beam while preserving a sufficient flux. Moreover, the beam is laminar and extremely well collimated, and the radiation source is—to a good extent—coherent, which opens the way to a wide range of innovative imaging techniques (see below).

On the detector side, the collaboration has developed an innovative digital detector,[3–6] which should replace conventional screen–film systems. This device consists of a silicon microstrip detector used in edge-on geometry, with radiation impinging on one of the thin sides of the silicon chip, instead of striking one of the large surfaces as occurs—for instance—in high energy physics experiments. In this way, the whole depth of the chip is made available for photon conversion, and thus an extremely high absorption efficiency is provided. This parameter is of primary importance in diagnostic radiology, since it results in the possibility of reducing the delivered dose. Moreover, the active surface of the device is, by construction, subdivided into pixels, whose dimensions are determined by the strip pitch in the horizontal direction and by the chip thickness in the vertical one. The three-layer detector layout is sketched in Fig. 1, and will be further discussed below. Each single pixel is read out by its own independent electronic chain, operating in single photon counting mode. This means that in principle image quality is limited only by the intrinsic quantum fluctuations of x-ray emission and absorption (Poisson statistics), i.e., the information extracted from the x-ray beam is maximized.

Due to the well-known advantages of digital imaging, digital radiology is rapidly becoming the new standard in nearly all fields;[7,8] in particular, flat panel detectors[9–12] are undergoing a widespread diffusion in the field of mammography. Nearly all these digital devices, however, are read out by charge integrating electronics, while further relevant improvements can be achieved by counting every single photon. In addition to the early research carried out by our collaboration, recently further research on single photon

[a]Author to whom correspondence should be addressed; electronic mail: olivo@trieste.infn.it

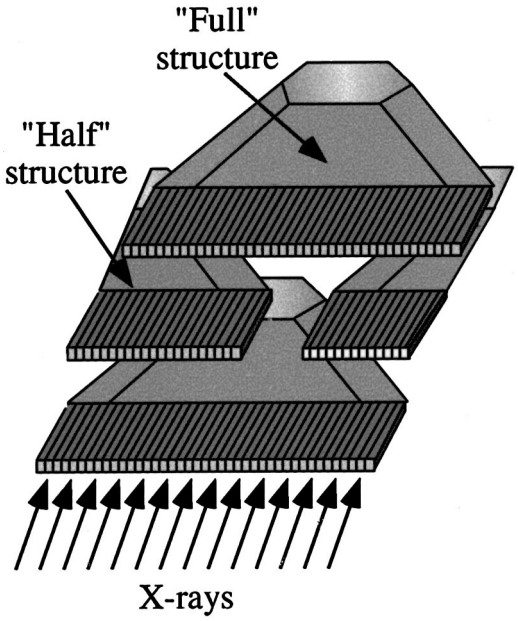

FIG. 1. Schematic layout of the SYRMEP/FRONTRAD three-layer detector assembly.

counting read-out electronics has been carried out by other groups,[13–15] and, furthermore, single photon counting systems have been produced by Sectra, SWE,[16] and by XCounter, SWE.[17]

Together with detector and read-out electronics development, new imaging modalities have been deeply investigated due to their high potentials in radiological applications. The most relevant example is probably given by phase contrast imaging which, based on the phase shifts suffered by the x-ray wavefield when crossing an object, provides the possibility of imaging details with the same absorption properties of the surrounding background. After pioneering experiments,[18–20] the possibility of applying this technique to diagnostic radiology, and in particular to mammography, was investigated.[21,22]

Another application to diagnostic radiology of phase imaging, called diffraction enhanced or diffraction imaging,[23,24] has also been investigated. This technique consists of using an analyzer crystal placed between the radiographed sample and the detector, while with ''phase contrast'' one usually refers to free Fresnel propagation of the x-ray wavefield between the sample and the detector.

Finally, scatter imaging and scatter tomography are currently taken into account by several authors,[25–29] and the fact that healthy and malignant breast tissue can be distinguished by means of their scattering signatures has been widely demonstrated.[30,31]

One of the main lines of research of our collaboration regards the implementation of all these techniques by means of the in-house developed silicon microstrip detector, since this would result in combining all the advantages brought by these imaging modalities with the ones of the SYRMEP/FRONTRAD detector, namely the very high efficiency resulting in a low delivered dose and the single photon counting capability allowing the detection of the smallest signals.

A three-layer prototype has already been developed and tested by the collaboration.[32,33] The knowledge achieved by developing this prototype has then been used to design another three-layer detector, with a minimized interlayer distance.

In the present article the performance evaluation of this device is described, and the possible simultaneous acquisition of several images obtained with different techniques is discussed.

II. MATERIALS AND METHODS

A. The beamline

All the herein described measurements were carried out at the SYRMEP beamline. The radiation beam is originated by one of the bending magnets of the ELETTRA storage ring, and the small source dimensions (about 0.14×1.1 mm^2), together with a source to sample distance of about 23 m, result in a high degree of spatial coherence. Two berillium windows located along the beam pipe allow the transportation of the beam itself from the storage ring ultrahigh vacuum to the experimental room, in air. The beam is monochromatized by means of a channel cut Si (1,1,1) crystal, allowing a 0.2% resolution in the energy range 8–35 keV. At the entrance of the experimental room, a micrometric precision tungsten slit system is used to shape the monochromatic beam. The maximum beam cross section is equal to 100 (width)$\times$4 [height, full width half maximum (FWHM)] mm^2. By means of the slit system mentioned above, any beam dimensions ranging from a few μm^2 to the maximum beam cross section are thus made available in the experimental hutch. Downstream of the slit system, and immediately upstream from the sample, a large area, nitrogen-fluxed, custom-built ionization chamber read out by a Keithley amperometer is used to monitor the incoming beam and thus to evaluate the dose delivered to the samples.

B. The image acquisition setup

Typically, the beam is shaped in such a way that its cross section equals the detector active area (50×0.3 or 100×0.3 mm^2 for single layer detectors, about 50×1 mm^2 for the three-layer prototype, as described below). Once the beam cross section and detector active surface have been matched, the beam and the detector are kept stationary and the two dimensional images are obtained by vertically scanning the samples through the laminar beam. The above beam to detector matching is obtained by means of a three-axis micrometric precision scanning device lodging the detector; a second, remotely controlled, micrometric precision vertical stage is used for scanning the sample through the beam.

With this image acquisition setup, small air gaps (a few cm) allow an almost complete removal of the scattered radiation from the acquired images.[6,34] This setup described above is used to acquire transmission images, based only on the absorption properties of the imaged object; slight changes in this setup allow the implementation of different phase imaging techniques.

First of all, the sample-to-detector distance has to be increased to about 2 m, to convert the small angular deviations of the photons due to phase shift effects into signals compatible with the detector aperture. Then, pixel size reduc-

tion by means of a slit system allows phase contrast imaging, since the detection of interference patterns connected with phase contrast imaging requires a small pixel size. Partial illumination of the detector active surface allows refraction imaging,[35] a technique providing imaging results similar to the ones given by diffraction imaging,[24] without requiring an analyzer crystal. Finally, shifting the detector active surface out of the primary beam opens the way to extremely small angle scatter imaging. All these techniques are described in detail in Refs. 29 and 35, and some examples of application will be given at the end of Sec. III.

C. The detector

An in-house developed acquisition software, written in *C* and running on a Pentium 200 PC with a LINUX operating system, reads out the detector while synchronizing this operation with the sample scanning. The detector layout has already been sketched above and is described in detail in Refs. 3–6 and 32–34.

In order to build the three-layer prototype, two ''full'' structures, featuring 256 channels each one having a width equal to 200 μm, and two ''half'' structures with 126 channels were built and stacked together as shown in Fig. 1. The ''half'' structures feature 126 instead of 128 channels because a guard ring was present in the outer part (with respect to Fig. 1) of these ''half'' devices, in order to avoid dramatic increases in the reverse dark current.

With this assembling scheme, the peculiar trapezoidal shape of the fan-out region allows a safe and simple wire bonding of each structure, without requiring any increase of the interlayer distance: the bonding regions of the upper and central layer are completely free, while above the same region of the lower layer a clearance equal to the thickness of one detector layer (300 μm) plus two interlayer distances (about 50 μm each, see below) is present.

Hence, the three-layer assembly technique follows the same main lines discussed in Refs. 32 and 33; particular care, however, was taken in the minimization of the interlayer distance. 50 μm thick kapton foils, with circular holes for glue dripping, were used as spacers; this allowed a substantial reduction of the interlayer distance with respect to the previous prototype. Furthermore, the kapton spacers and the siliconic glue prevent any electrical contact between the detector layers. The final assembly was realized by MIPOT;[36] a series of tests carried out on detector-shaped 300 μm thick pieces of glass allowed the realization of the final assembly with an interlayer distance practically equal to the kapton spacers, without causing any damage to the detector components.

D. The samples

A bar pattern test object (a lead mask in which several line patterns with different micrometric spacing have been carved, BPTO in the following) was used for spatial resolution evaluation. A sharp edge of the same mask was used for point spread function (PSF) evaluation, as well as for detector active surface characterization and interlayer distance estimation (see below).

A ''contrast-detail (CD) phantom'' (i.e., a Plexiglas slab containing disks of different thickness and diameter) was used for contrast resolution evaluation.

Finally, a small fish was used to check the image quality obtainable with the different techniques on a biological sample.

III. RESULTS AND DISCUSSION

A. Active surface characterization

After shaping the beam and aligning it with respect to the detector active surface, a sharp full absorbing edge was scanned in front of the detector in order to characterize its active surface. By horizontally scanning the edge, the correspondence between channels of different layers was checked, while a vertical scan of the edge provides an estimate of the interlayer distance.

1. Horizontal characterization: Channel correspondence

When the first three-layer prototype[32,33] was assembled, the physical edges of the silicon chips were laterally aligned. This procedure gave unsatisfactory results, since, due to the presence of a guard ring on the outer side of the chips, the distance between the physical edge of the chip and the first strip implant was not exactly the same for all chips. As a result, corresponding channels of different layers were not perfectly overlapping.

In the assembly of the herein discussed second prototype, the first implanted strips of every layer were aligned one with respect to the other. Furthermore, when assembling the central layer, the distance between the last strip of one half structure and the first strip of the other one was kept equal to two detector channels (400 μm). In this way, in the middle of the central layer a dead region corresponding to two detector channels was present, but the alignment of the remaining channels with respect to the other layers was not compromised.

The effectiveness of this approach was tested by means of the synchrotron beam. The beam energy was set equal to 20 keV. The counts of each channel were registered while a sharp edge was horizontally scanned with 10 μm steps in front of the detector: in this way, an (horizontal) edge response function (ERF)[37,38] was acquired for every channel. By numerically differentiating the ERF for every channel, the correspondent horizontal line spread function (LSF) (i.e., the curve obtained by integrating the PSF along one direction) is achieved. By fitting these LSFs the centroid of each curve, which gives a good estimate of the channel position, is obtained. In this way, the above discussed alignment was checked with a precision of about 10%. This study provided a ''correspondence map'' between channels belonging to different layers, used in the following to combine the information on the same sample coming from the different detector layers.

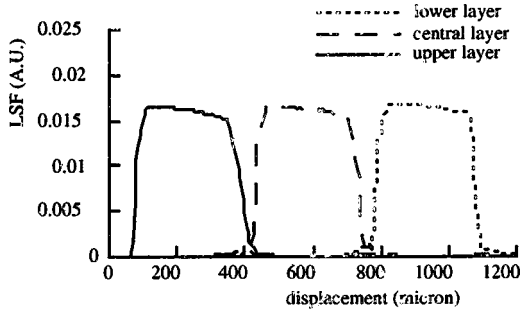

FIG. 2. Vertical LSF of three corresponding pixels belonging to the three detector layers. Error bars, not reported on the graph, are of about 1%.

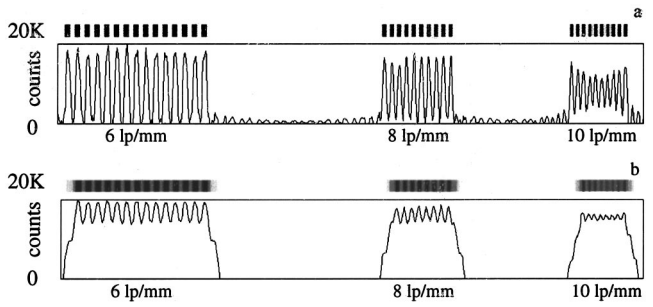

FIG. 3. Images of a bar pattern test object, obtained by scanning the sample with a step (20 μm) smaller than the pixel size (300 μm): (a) the processed image featuring a spatial resolution increase, (b) the raw image.

2. Vertical characterization: Interlayer distance

The same technique was used to measure the interlayer distance. In this case, the full absorbing edge was scanned in front of the detector vertically, with a scanning step equal to 5 μm. The reduction in the scanning step is due to the fact that from this measurement the vertical LSF of the detector is obtained, and this function will be used to increase the spatial resolution of the device (see below). Thus, we wanted to know this quantity with a maximum error of 10 μm. After obtaining the vertical ERFs for all channels, the numerical derivative provides the vertical LSFs. The LSFs of three corresponding channels belonging to different detector layers as a function of the scanning step (i.e., of the vertical position) are shown in Fig. 2. By evaluating the position of the centroids of each curve, one can estimate the interlayer distances. The obtained results are 40 ± 10 μm for the distance between the upper and central layer, and 50 ± 10 μm for the one between the central and lower layer.

The procedure has been repeated for several triplets of corresponding channels all along the detector active surface, and the same results were always obtained. This proves that the interlayer distance is held constant throughout the entire detector active surface, i.e., the detector layers are parallel one with respect to the other within the experimental uncertainty.

B. Spatial resolution

The spatial resolution has been intensively studied along the vertical direction, i.e., the direction of the scanning of the samples through the beam. When images are acquired by means of a scanning system, it is in fact possible to achieve an enhanced spatial resolution with respect to the intrinsic one along the scanning direction: this is obtained by scanning the samples with a step smaller than the pixel size. In this way, a convolution between the image and the pixel LSF is acquired, and an off-line filtered deconvolution procedure can provide an image in which the spatial resolution is determined by the scanning step rather than by the pixel size.[39]

An example is given in Fig. 3, where a part of the BPTO has been acquired with a scanning step of 20 μm. The processed image [Fig. 3(a)] is compared to the raw data [Fig. 3(b)]; as it can be seen, also the smallest details are resolved when the deconvolution algorithm is applied.

The intrinsic resolution of the device is fully described by the functions shown in Fig. 2. It has to be noted that the three curves shown in Fig. 2 are not identical: the FWHM is equal to 310 ± 10, 315 ± 10, and 290 ± 10 μm for the upper, the central, and the lower layer, respectively. The above discrepancy is probably due to a physical difference in the thickness of the three silicon chips (the two ''half structures'' forming the central layer were obtained from the same silicon wafer). By Fourier transforming the LSF, the intrinsic modulation transfer function (MTF)[37,38] of the device is obtained. On the other hand, the MTF can also be directly obtained from BPTO images; in fact, MTF evaluation from raw-data images like the one shown in Fig. 3(b) and from Fourier transformation of the LSF leads to the same results.[39] On the other hand, processed images like the one shown in Fig. 3(a) allow the estimation of the enhanced MTF, and its increase with respect to the intrinsic one can be evaluated.

Figure 4 shows the intrinsic MTF evaluated from the unprocessed BPTO image. The MTF values extracted from each layer are reported, and the small discrepancies among them are consistent with the above discussed differences in the LSFs. Another BPTO image has been acquired at about one third of the statistics ($\sim$3300 photons per pixel per acquisition step instead of 10 000), and an image with a statistic of about 10 000 photons per pixel has then been reconstructed by summing up the information provided by each layer, taking into account the interlayer distances evaluated as discussed above. The MTF values extracted from this reconstructed image are also reported on the graph: as it can be seen, these values always lie in the range of the values extracted from the single layer images. This demonstrates that no spatial resolution is lost when information obtained from

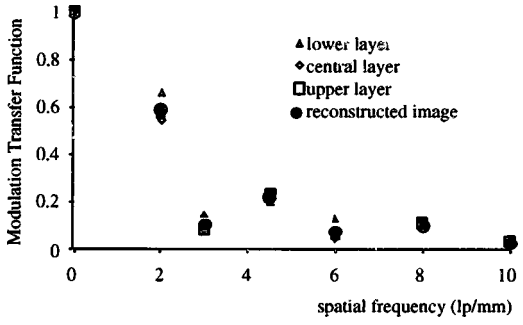

FIG. 4. Intrinsic MTF of the three detector layers, together with the MTF evaluated from an image obtained by combining the data collected by each detector layer (''reconstructed image''). Error bars, not reported on the graph, are of about 10%.

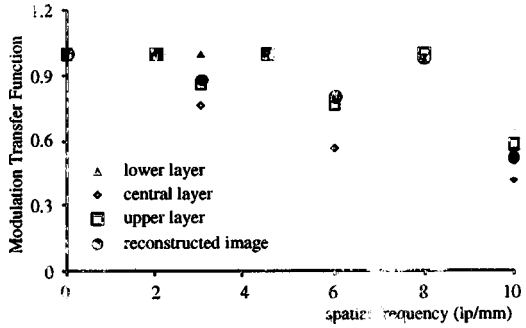

FIG. 5. Enhanced MTF of the three detector layers, obtained by means of the filtered deconvolution procedure. The MTF evaluated from an image obtained by combining the data collected by each detector layer ("reconstructed image") is also shown. Error bars, not reported on the graph, are of about 10%.

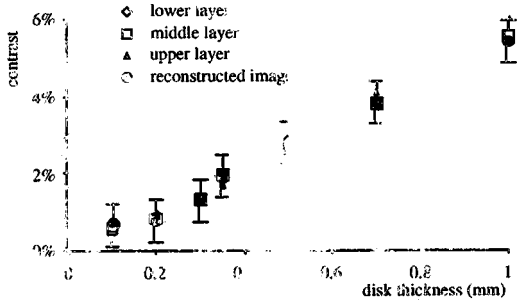

FIG. 7. Contrast values evaluated for each of the disks shown in Fig. 6. Rhombs, squares, and triangles represent the values extracted separately from each detector layer, while circles stand for the values evaluated from the "reconstructed image," obtained by combining the information coming from each layer.

the three detector layers is combined, while providing at the same time a crosscheck on the reliability of the interlayer distance evaluation.

The same procedure has been applied to the processed image [a part of which is shown in Fig. 3(a)], and the results are shown in Fig. 5. As it can be seen, the MTF values are much higher than the ones shown in Fig. 4, and they closely approach the theoretical MTF of a pixel having dimensions equal to 20 μm.[39]

The only exception regards the points where the intrinsic MTF values are very close to zero. For a "perfect" 300 μm pixel, i.e., a pixel the LSF of which is a 300 μm wide box function, these zero values would be at 3.33 and 6.66 lp/mm, and it would be impossible to restore these spatial frequencies.[39] For a real pixel, where the ideal "box" shape of the LSF is rounded off, the MTF at the above frequency is very small but not equal to zero, so a partial restoration of those frequencies is possible in the processed image. This explains why the MTF shown in Fig. 5 has local minima at the above frequencies.

The MTF has also been evaluated from an image obtained by summing up images taken from each layer at one third of the statistics, and again the reconstructed image MTF always lies within the single layer values. Hence, no resolution loss occurs when information collected by the three layers is combined, even when the spatial resolution enhancement procedure is applied.

C. Contrast resolution

As mentioned above, the single photon counting capability of the readout electronics maximizes the contrast resolution. For contrast resolution evaluation, several images of a CD phantom (see Sec. II D) have been taken; one of these images (taken at 20 keV) is shown in Fig. 6. The thinnest disk, on the right hand side of the image, has a contrast of about 0.5%, while with conventional screen–film systems the minimum detectable contrast ranges from 2%–3%.

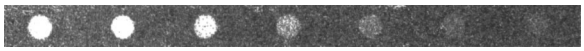

FIG. 6. Image of the contrast-detail phantom, used for contrast resolution evaluation.

The contrast values measured for each disk shown in Fig. 6 are reported in Fig. 7 for each detector layer. As it was expected, the evaluated contrast values are the same within the experimental uncertainty for the three detector layers.

As already done when the spatial resolution was evaluated, an image was acquired with one third of the statistics (~3300 photons/pixel/acquisition step instead of 10 000), and an image with a statistic of about 10 000 photons per pixel was then reconstructed by summing up the information coming from each layer. The contrast of each disk was also evaluated in the reconstructed image, and the obtained results are reported in the graph of Fig. 7. As it can be seen, the contrast values measured from the reconstructed image always lay within the values of the single layer images, which means that no contrast resolution is lost when the information coming from each detector layer is combined to form a single image.

D. Imaging results

Finally, the imaging capabilities of the system have been tested on a biological sample (a small fish, length ~4 cm); some examples of the acquired images are shown in Fig. 8. Figure 8(a) shows the absorption image: one of the 300 μm thick silicon layers was fully illuminated by the incoming beam, and the fish was vertically scanned in front of the detector, with a sample-to-detector distance of a few cm. As a result, a low-dose, high-contrast digital image is obtained.

Figure 8(b) shows an image obtained with a sample to detector distance of about 2 m, and with the vertical dimension of the pixel reduced down to about 100 μm by means of a slit carved in a copper slab. As a result of the increased sample to detector distance and of the reduced pixel dimensions, phase contrast effects are detected, superimposed to the absorption image. Due to the presence of these phase effects, the contrast of all details is strongly increased in the image. This is apparent in the head of the fish, which is more structured than the rest of the body; nearly all the ribs are visible and the overall image quality is clearly increased both in terms of contrast and of detail visibility.

Figure 8(c) shows an image obtained with a sample to detector distance of about 2 m, without the copper slit, but illuminating only a part (close to the physical edge)[35] of the detector active surface.

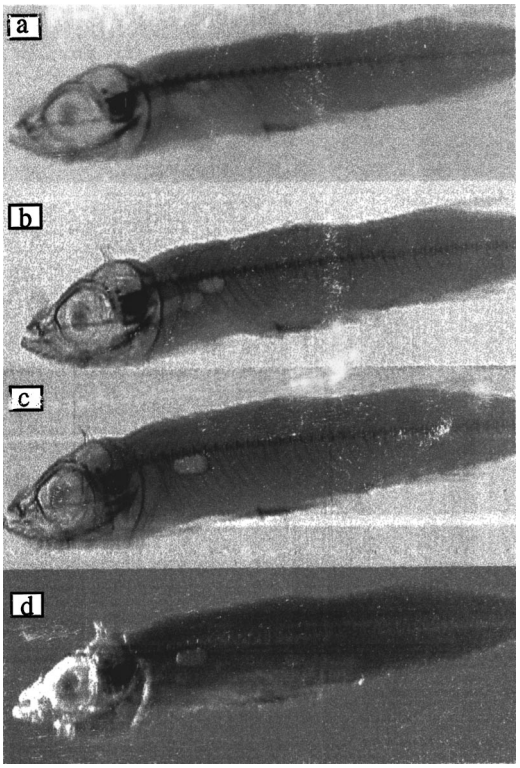

FIG. 8. Images of a small fish (length ~4 cm). (a), (b), (c), and (d) show the absorption, the phase contrast, the refraction, and the scatter image, respectively.

In this way, a digital refraction image[35] is acquired: the overall image quality is similar to the one shown in Fig. 8(b), and some details show an even higher contrast. This technique allows the acquisition of images with phase contrast quality even when detectors with relatively large active surfaces are used.

Finally, Fig. 8(d) shows an extremely small angle scatter image[29] of the sample: it has been obtained by moving the beam completely out of the detector active surface, with a distance of about 50 μm between the upper limit of the detector active surface and the lower limit of the beam. Also in this case, the sample to detector distance was of about 2 m, hence, photons scattered in the angular range between about 25 and 175 μrad were detected. The image appears quite different with respect to the previous ones, but the contrast of some details is further enhanced (in some cases also of 1 order of magnitude). As discussed in Ref. 29, this imaging modality can provide complementary information on the imaged sample with respect to the other techniques, and, most of all, can be implemented at no dose expense: one detector layer can be used to detect the scattered radiation while the other ones are illuminated by the primary beam. In particular, with a three-layer detector one could acquire three complimentary images with a single scan of the sample through the beam. This would be done by illuminating the entire central layer and only a part of one of the outer layers, leaving the third layer completely out of the primary beam.

[1] F. Arfelli *et al.*, Rev. Sci. Instrum. **66**, 1325 (1995).
[2] F. Arfelli *et al.*, Phys. Medica **XIII**, 7 (1997).
[3] F. Arfelli *et al.*, Phys. Medica **IX**, 229 (1993).
[4] F. Arfelli *et al.*, Nucl. Instrum. Methods Phys. Res. A **353**, 366 (1994).
[5] F. Arfelli *et al.*, IEEE Trans. Nucl. Sci. **44**, 874 (1997).
[6] F. Arfelli *et al.*, Phys. Med. Biol. **42**, 1565 (1997).
[7] M. J. Yaffe and J. A. Rowlands, Phys. Med. Biol. **42**, 1 (1997).
[8] S. A. Feig and M. J. Yaffe, Radiographics **18**, 893 (1998).
[9] L. E. Antonuk, J. Yorkston, W. Huang, J. H. Siewerdsen, J. M. Boudry, Y. El-Mohri, and M. V. Marx, Radiographics **15**, 993 (1995).
[10] R. Fahrig, J. A. Rowlands, and M. J. Yaffe, Med. Phys. **22**, 153 (1995).
[11] W. Zhao, I. Blevis, S. Germann, J. A. Rowlands, D. Waechter, and Z. Huang, Med. Phys. **24**, 1834 (1997).
[12] J. Rowlands and S. Kasap, Phys. Today 24 (1997).
[13] E. Beuville, B. Cederstrom, M. Danielsson, L. Luo, D. Nygren, E. Oltman, and J. Vestlund, Nucl. Instrum. Methods Phys. Res. A **406**, 337 (1998).
[14] D. G. Gobbi, M. S. Dixit, J. Dubeau, and P. C. Johns, Phys. Med. Biol. **44**, 1317 (1999).
[15] B. Hilt, P. Fessler, and G. Prevot, Nucl. Instrum. Methods Phys. Res. A **442**, 38 (2000).
[16] For a description of the system, see www.sectra.se
[17] www.xcounter.se
[18] A. Snigirev, I. Snigireva, V. Kohn, S. Kuznetsov, and I. Schelokov, Rev. Sci. Instrum. **66**, 5486 (1995).
[19] T. J. Davis, D. Gao, T. E. Gureyev, A. W. Stevenson, and S. W. Wilkins, Nature (London) **373**, 595 (1995).
[20] S. W. Wilkins, T. E. Gureyev, D. Gao, A. Pogany, and A. W. Stevenson, Nature (London) **384**, 335 (1996).
[21] M. Di Michiel *et al.*, in *Medical Applications of Synchrotron Radiation*, edited by M. Ando and C. Uyama (Springer, Tokyo, 1998), pp. 78–82.
[22] F. Arfelli *et al.*, Phys. Med. Biol. **43**, 2845 (1998).
[23] D. Chapman *et al.*, Phys. Med. Biol. **42**, 2015 (1997).
[24] F. Arfelli *et al.*, Radiology **215**, 286 (2000).
[25] G. Harding, J. Kosanetzky, and U. Neitzel, Med. Phys. **14**, 515 (1987).
[26] R. J. Leclair and P. C. Johns, Med. Phys. **25**, 1008 (1998).
[27] U. Kleuker, P. Suortti, W. Weyrich, and P. Spanne, Phys. Med. Biol. **43**, 2911 (1998).
[28] R. A. Lewis *et al.*, Proc. SPIE **3770**, 32 (1999).
[29] A. Olivo *et al.*, Phys. Med. Biol. **47**, 469 (2002).
[30] S. H. Evans, D. A. Bradley, D. R. Dance, J. E. Bateman, and C. H. Jones, Phys. Med. Biol. **36**, 7 (1991).
[31] G. Kidane, R. D. Speller, G. J. Royle, and A. M. Hanby, Phys. Med. Biol. **44**, 1791 (1999).
[32] F. Arfelli *et al.*, Informacije MIDEM **29**, 26 (1999).
[33] F. Arfelli *et al.*, Nucl. Phys. B **78**, 592 (1999).
[34] F. Arfelli *et al.*, Radiology **208**, 709 (1998).
[35] A. Olivo *et al.*, Med. Phys. **28**, 1610 (2001).
[36] MIPOT S.p.A., Via Corona 5, 34071 Cormons (GO), Italy.
[37] H. Fujita, D. Tsai, T. Itoh, K. Doi, J. Morishita, K. Ueda, and A. Ohtsuka, IEEE Trans. Med. Imaging **11**, 34 (1992).
[38] B. H. Hasegawa, *The Physics of Medical X-Ray Imaging* (Medical Physics, Madison, WI, 1990).
[39] A. Olivo *et al.*, Med. Phys. **27**, 2609 (2000).